European Journal of Applied Sciences – Vol. 12, No. 06
Publication Date: December 25, 2024
DOI:10.14738/aivp.1206.18060.
Sorescu, M., Adams, L., Tolea, F., Sofronie, M., Kelly, J. C., & Aitken, J. A. (2024). Mechanochemical Synthesis and Characterization of Samarium Oxide-Hematite Magnetic Ceramic Nanostructures. European Journal of Applied Sciences, Vol - 12(06). 693-708.

Mechanochemical Synthesis and Characterization of Samarium Oxide-Hematite Magnetic Ceramic Nanostructures

Monica Sorescu
Duquesne University, Department of Physics,
Fisher Hall, Pittsburgh, PA 15282, United States

Lona Adams
Duquesne University, Department of Chemistry and Biochemistry, Mellon Hall, Pittsburgh, PA 15282, United States

Felicia Tolea
National Institute of Materials Physics,
Bucharest-Magurele, 077125, Romania

Mihaela Sofronie
National Institute of Materials Physics,
Bucharest-Magurele, 077125, Romania

Jordan C. Kelly
Duquesne University, Department of Chemistry and Biochemistry, Mellon Hall, Pittsburgh, PA 15282, United States

Jennifer A. Aitken
Duquesne University, Department of Chemistry and Biochemistry, Mellon Hall, Pittsburgh, PA 15282, United States

ABSTRACT

Mixed-oxide nanostructures of the type xSm_2O_3-(1-x) a-Fe_2O_3 (x=0.1 and 0.5) were synthesized by mechanochemical activation for ball milling times of 0, 2, 4, 8 and 12 hours. The 0-h Mössbauer spectrum was analyzed with a sextet characteristic to hematite. A second sextet with a lower value of the hyperfine magnetic field was assigned to samarium-doped hematite. An additional quadrupole-split doublet, whose abundance showed a general trend to increase with the ball milling time, was attributed to superparamagnetic samarium iron perovskite (samarium orthoferrite) phase. The X-ray diffraction (XRD) patterns for the equimolar composition were dominated by the diffraction peaks of $SmFeO_3$ after 12 h of milling. The hysteresis loops recorded at 5 K and an applied magnetic field of 5 T exhibited higher values of the magnetization than the similar ones measured at 300 K, but did not saturate at this field strength. The coercive field values showed a decrease with decreasing the particle size after prolonged milling. The zero-field-

cooling-field-cooling (ZFC-FC) measurements performed at 200 Oe and 5-300 K were consistent with an increase in magnetization with ball milling time. The Tauc plots derived from the optical diffuse reflectance spectra showed that the samples were semiconductors with a band gap of ~2.1 eV.

Keywords: oxides, Mössbauer spectroscopy, magnetic properties.

INTRODUCTION

Samarium ion Sm^{3+} is a paramagnetic light rare earth ion with extremely interesting properties when introduced in various materials systems [1-19]. Thus, Sm doped Ba-Co hexaferrites were found to exhibit decreased specific saturation magnetization, coercivity and retentivity values with increasing concentration of Sm ions in the Ba-Co lattice, along with excellent values of the squareness ratio [1]. Enhanced ferromagnetic nature was evidenced in Ce-Sm doped Co-Ni ferrite nanoparticles and the presence of superparamagnetic relaxation with a blocking temperature (T_B) higher than room temperature was inferred from Mössbauer spectra [2]. Samarium doped magnetite nanoparticles synthesized using the polyol method were found to present superparamagnetism at room temperature and anhysteretic behavior [3]. The crystal structure, microstructure and magnetic properties of cobalt ferrite could be tailored by introducing small amounts of gadolinium or samarium [4]. XRD and Mössbauer measurements confirmed the presence of hematite and samarium iron perovskite (samarium orthoferrite, $SmFeO_3$) in calcined nickel-copper-zinc mixed ferrite nanoparticles [5]. The semiconductive nature of $SmFeO_3$ was confirmed in [15] by electric conductivity measurements and its weak ferromagnetic behavior at room temperature was evidenced by magnetic and Mössbauer studies. This was due to Dzyaloshinsky-Moriya antisymmetric exchange interaction mechanism, but it should be emphasized that these results were obtained for particles 0.55 mm in size.

Hematite (a-Fe_2O_3) has been the subject of intense theoretical and experimental investigations, due to its use as a magnetic, semiconductor and catalytic material. Doping hematite with various transition metal and rare earth elements was found to result in an improvement of its electrochemical and photocatalytical properties [20-26]. Mechanochemical activation by high-energy ball milling played a significant role in the synthesis of various Sm-doped systems [6, 12, 17-19]. Recently, the ball milling technique was key to obtaining garnet-graphene nanocomposites [27] and crucial to determine the formation of skyrmion phase in the Fe-Co-Si system [28]. Moreover, mechanochemical activation was used to synthesize mixed-oxide nanostructures of the type xGd_2O_3-(1-x) a-Fe_2O_3 [29] and xNd_2O_3-(1-x) a-Fe_2O_3 [30] with the presence of solid solutions in the former and absence of solid solutions in the latter system.

In the present study we investigate the structural, magnetic and optical properties of the xSm_2O_3-(1-x) a-Fe_2O_3 system with molar concentration x=0.1 and 0.5, obtained by mechanochemical activation at different ball-milling times. Our investigation aims at determining the phase sequence and mutual solubility of the mixed oxides as a function of processing parameters and is conducted by Mössbauer spectroscopy, X-ray diffraction (XRD), magnetic measurements (hysteresis loops and zero-field-cooling-field-cooling, ZFC-FC) and optical diffuse reflectance spectroscopy. Mixed oxides have potential applications in sensing, catalysis and flexible electronics.

MATERIALS AND METHODS

Nanoparticles of xSm_2O_3-(1-x) a-Fe_2O_3 (x=0.1 and 0.5) were obtained by mechanochemical activation of precursor powders of hematite and samarium oxide with particle sizes of 50 and 90 nm, respectively (Alfa Aesar). The powders were mixed manually using a mortar and pestle and introduced in a SPEX 8000 mixer mill and ground for time periods ranging from 0 to 12 hours. The powder to ball mass ratio was 1:5.

The room-temperature transmission Mössbauer spectra were recorded using a SeeCo constant accelerator spectrometer equipped with a 25 mCi ^{57}Co gamma ray source in a Rh matrix. All spectra were analyzed by least-squares fitting using the WINORMOS package of programs in the assumption of Lorentzian lineshapes.

The microcrystalline sample was ground well and deposited onto a zero-background silicon wafer. Powder X-ray diffraction data were collected using a Malvern Panalytical Empyrean 3 multipurpose powder X-ray diffractometer with an X'cellerator detector operating in Bragg–Brentano geometry and using Cu $K\alpha$ radiation, λ = 1.541871 Å. The tube was energized using 45 kV and 40 mA. Data were collected from 5 to 100° 2θ in steps of 0.0167° at a scan speed of 0.023537° s^{-1}. A 0.04 rad soller slit and a 2° anti-scatter slit were used on the incident side of the beam, while the diffracted beam optics consisted of a 0.04 rad soller slit, a programmable anti-scatter slit, and a nickel filter. Phase identification of crystalline components was carried out using the *X'Pert HighScore Plus* software package and the International Centre for Diffraction Data (ICDD) powder diffraction file (PDF) database.

Magnetic property measurements were performed using a superconductor quantum interference device (SQUID) magnetometer with a 5 T magnetic field for recording the hysteresis loops at 300 and 5 K and a 200 Oe magnetic field for the zero-field-cooling-field-cooling (ZFC-FC) measurements in the 5-300 K temperature range.

A Varian Cary 5000 UV–Vis–NIR spectrophotometer coupled with a diffuse reflectance accessory was used to collect data from 2500 to 200 nm at a rate of 600 nm min^{-1}. The 100% reflectance standard was $BaSO_4$ (Fisher Scientific, 99.92%). The sample was ground and pressed on top of the reference that was preloaded in the sample cup. Reflectance data were converted to absorption by employing the Kubelka–Munk equation.

RESULTS AND DISCUSSION

Mössbauer Spectroscopy

In order to obtain local-probe information on the structural and magnetic properties of samarium oxide-hematite ceramic nanostructures, Mössbauer spectroscopy was employed.

Figures 1-2 (a)-(e) show the room-temperature transmission Mössbauer spectra of the xSm_2O_3-(1-x) a-Fe_2O_3 nanoparticles system for molar concentration x=0.1 and 0.5 and ball milling times (BMT) of 0, 2, 4, 8 and 12 hours, respectively. The refined values of the hyperfine parameters extracted from these spectra by nonlinear least-squares fitting are listed in Table 1. The spectra in Figures 1-2 (a) were analyzed considering one six-line pattern, with the magnetic hyperfine field (B_{hf}) of 50.7 T, characteristic to hematite.

Analysis of the Mössbauer spectra in Figures 1-2 (b)-(e) required the consideration of a second sextet, with a magnetic hyperfine field smaller than that of hematite. This sextet occurs due to substitutions of Fe atoms by Sm atoms and can be understood in terms of the model of local atomic environment. Indeed, it is known that the substitution of Fe atoms by nonmagnetic ions lowers the magnetic hyperfine field at the Fe sites. Consequently, this sextet was assigned to samarium-doped hematite.

The dependance of the magnetic hyperfine field values of the two sextets on the ball milling time is consistent with the formation of a limited solid solution in the studied samples. The ionic radius of the Sm^{3+} ions with six coordination numbers is 0.958 Å, while that of the Fe^{3+} ions is 0.645 Å. Due to this difference in the ionic radii, a higher level of substitution cannot occur and only a limited solid solution is obtained.

The Mössbauer spectra in Figures 1 (b)-(e) and 2 (b)-(e) were analyzed by considering an additional quadrupole-split doublet, with the quadrupole splitting in the range 0.5-0.8 mm/s, which could be assigned to superparamagnetic samarium iron perovskite (samarium orthoferrite), $SmFeO_3$. Samarium orthoferrite is known to exhibit two antiferromagnetically-coupled sublattices for particles of the order of a few micrometers [15], but in the present study the nanoparticles of samarium orthoferrite are too small to be magnetic at room temperature, such that superparamagnetism occurs. The reduced particle size due to prolonged milling is translated into a quadrupole-split doublet in the Mössbauer spectra.

Table 1: Mössbauer parameters of the $xSm_2O_3*(1-x)$ a-Fe_2O_3 system: isomer shift d (relative to Fe), quadrupole splitting D, quadrupole shift 2e, magnetic hyperfine field B_{hf}, relative areas and assignment of sites.

Sample (x)	BMT (h)	δ (mm/s)	Δ (mm/s)	2ε (mm/s)	Bhf (T)	Relative areas (%)	Assignment of sites
0.1	0	0.36		-0.21	50.7	100	Fe_2O_3
	2	0.36		-0.19	51.2	43.83	Fe_2O_3
		0.36		-0.22	49.8	55.37	Sm: Fe_2O_3
		0.16	0.53			0.8	$SmFeO_3$
	4	0.37		-0.2	51	48.12	Fe_2O_3
		0.34		-0.2	48.6	50.08	Sm: Fe_2O_3
		0.16	0.64			1.8	$SmFeO_3$
	8	0.36		-0.21	51.2	54.04	Fe_2O_3
		0.36		-0.21	50	44.93	Sm: Fe_2O_3
		0.24	0.30			1.03	$SmFeO_3$
	12	0.36		-0.2	51.1	66.8	Fe_2O_3
		0.35		-0.21	48.6	30.80	Sm: Fe_2O_3
		0.27	0.49			2.4	$SmFeO_3$
0.5	0	0.36		-0.32	50.9	100	Fe_2O_3
	2	0.37		-0.2	51.4	35.83	Fe_2O_3
		0.35		-0.21	50.3	61.71	Sm: Fe_2O_3
		0.18	0.48			2.46	$SmFeO_3$
	4	0.36		-0.2	50.8	33.11	Fe_2O_3

		0.26		-0.26	45.9	42.29	Sm: Fe_2O_3
		0.40	0.97			2.46	$SmFeO_3$
	8	0.36		-0.19	51.1	20.76	Fe_2O_3
		0.35		-0.19	49.4	37.99	Sm: Fe_2O_3
		0.29	0.98			41.25	$SmFeO_3$
	12	0.35		-0.22	50.8	16.41	Fe_2O_3
		0.37		-0.16	49.8	47.69	Sm: Fe_2O_3
		0.37	0.77			35.90	$SmFeO_3$
Errors:		±0.1	±0.1	±0.1	±0.5	±0.1	

Table 1 also presents the dependence of the relative abundance of the quadrupole-split doublet as a function of the ball milling time for both values of the molarities used. It can be inferred that the doublet abundance increases with increasing the milling time and reaches 41.25% for the sample with x=0.5 ball-milled for 8 hours. The occurrence of the samarium iron perovskite during the mechanochemical activation process can be modeled by considering the reaction $Sm_2O_3+Fe_2O_3 \rightarrow 2SmFeO_3$, which is assumed to be induced by the high-energy ball milling performed.

X-ray Diffraction (XRD)

To complement the Mössbauer spectroscopy investigations on the phase composition of the milled samples, X-ray diffraction (XRD) measurements have also been performed. The XRD patterns of the xSm_2O_3-(1-x) a-Fe_2O_3 nanoparticles system for x=0.5 and ball milling times of 0, 2, 4, 8 and 12 hours, respectively are presented in Figure 3 (a)-(e). The diffractogram in Figure 3 (a) is consistent with diffraction peaks from a-Fe_2O_3 (PDF card 01-089-0597) and Sm_2O_3 (PDF card 01-076-3181) oxides, which correspond to the original starting material before ball milling. It can be inferred that the peaks of the samarium perovskite appear (PDF card 01-074-1474) after exposure to mechanochemical activation. The pattern of $SmFeO_3$ peaks dominates the XRD diffractogram after 12 h of exposure to high-energy ball milling. These results are in good, qualitative agreement with the Mössbauer findings presented in the previous section.

Magnetic Measurements

In order to complement the local-probe information obtained by Mössbauer spectroscopy, magnetic measurements were also performed. Figures 4 and 5 (a)-(e) show the hysteresis loops recorded at 5 K and respectively, 300 K with an applied magnetic field of 5 T (1T=10,000 Oe) for the equimolar composition samples (x=0.5), ball-milled for 0-12 h. It can be seen that saturation is not reached even in the magnetic field of 5 T. This is due to the paramagnetic contribution from the samarium orthoferrite phase and a weak ferromagnetic component due to hematite. The magnetic state of hematite is antiferromagnetic with the Neel temperature T_N=960 K [20-25]. Specific to hematite is the fact that its two magnetic sublattices have equal moment and antiparallel orientation below the Morin temperature, T_M=262 K, for pure hematite [25]. At temperatures higher than the Morin temperature, the two sublattices are slightly canted, leading to weak ferromagnetism.

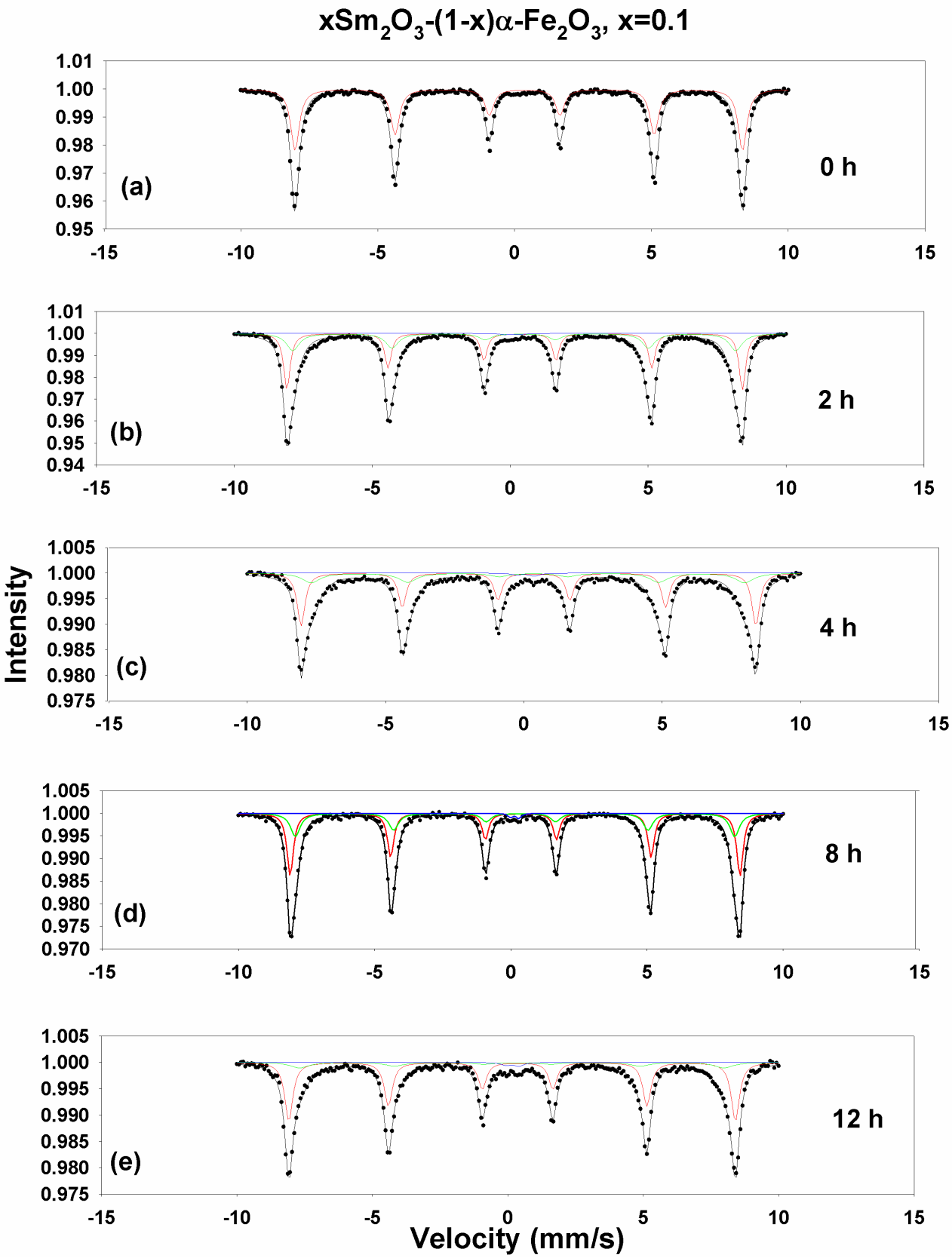

Fig. 1: Mössbauer spectra for x=0.1 and BMT of 0-12 h.

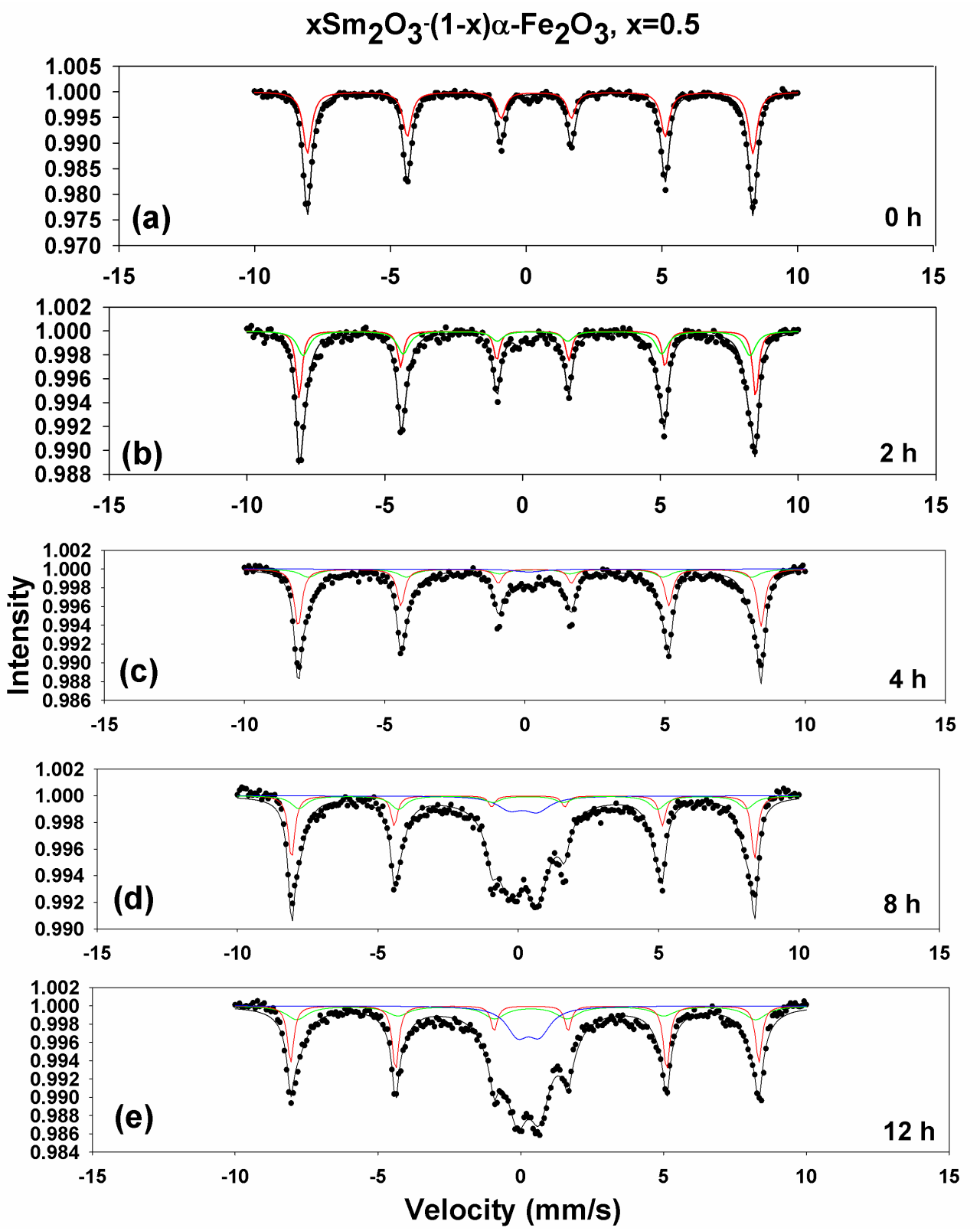

Fig. 2: Mössbauer spectra for x=0.5 and BMT of 0-12 h.

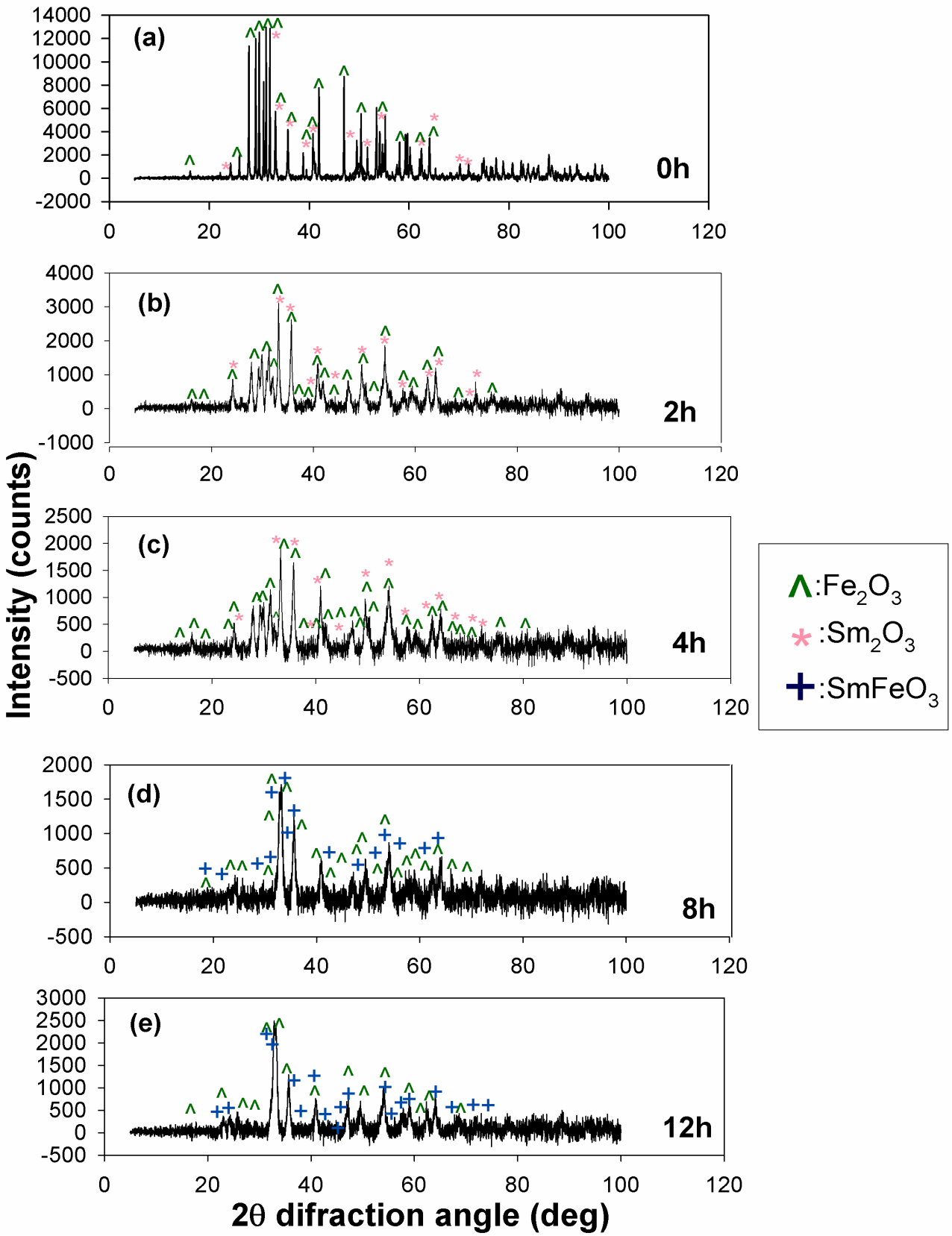

Fig. 3: XRD patterns for x=0.5 and BMT of 0-12 h.

At 300 K, the values of the magnetization increase slightly from 1 to 1.5 emu/g, with the maximum value corresponding to the sample ball-milled for 8 h. At 5 K, the values of the magnetization are higher than those at 300 K, ranging from 2-3 emu/g, with the maximum corresponding to the 8 h milled sample. The coercive field values are in the range of 180-482 Oe at 5 K and 140-390 Oe at 300 K, showing a decrease with decreasing the particle size after prolonged milling.

Figure 6 (a)-(e) shows the zero-field-cooling-field-cooling (ZFC-FC) curves recorded for the samarium oxide-hematite system (x=0.5) with an applied magnetic field of 200 Oe in the temperature interval 5-300 K, after having been exposed to milling for times of 0-12 h. As the milling time increases, the average crystallite size decreases and the hematite Morin temperature takes lower values, which are spread over a temperature interval. For these reasons the transformation resembles an incline instead of a step. It can be seen that the values of the magnetization on the FC curve (upper curve) increase steadily with ball milling time, from 0.035 emu/g for the 0-h sample to 0.08 emu/g for the 12-h milled sample. These results show that the values of the magnetic parameters can be controlled by the ball milling time employed.

Optical Diffuse Reflectance Spectroscopy

Optical diffuse reflectance spectroscopy measurements were performed in order to characterize the optical property changes induced by mechanochemical activation in the samarium oxide-hematite system. Figure 7 (a) shows the optical absorption spectra of the samarium oxide-hematite equimolar mixture as a function of energy over the UV-VIS-NIR spectral range for all milling times employed. For the starting material, hematite has a band gap of 1.9-2.2 eV in the visible region, while samarium oxide has absorption bands at 4.47 and 3.03 eV in the ultraviolet-visible region [31-33]. For the ball-milled material, it can be seen that the absorbance is considerably enhanced and broadened, an effect we believe to result from the substitution of Sm ions for Fe. Since the 2.2 eV transition in hematite is indirect, a plot of $(aE)^2$ as function of energy (eV) is able to yield the band gap of the compound, according to the Tauc plots [32]. Indeed, it can be observed in Figure 7 (b) that the intercepts give a value of ~2.1 eV for the band gap; moreover, this value is independent of the milling time employed. Indeed, it can be seen in this figure that there is no absorption below 2.1 eV for all milling times, while above the band gap there is a broad absorption that depends on the milling time employed. These results show that the samarium oxide-hematite mixed-oxide nanostructures have semiconductor properties.

CONCLUSIONS

In this study we successfully synthesized the compositional series xSm_2O_3-(1-x)a-Fe_2O_3 at two different molarities (x=0.1 and 0.5) by mechanochemical activation and characterized its structural, magnetic and optical properties as function of molarity and ball milling time by Mössbauer spectroscopy, X-ray diffraction, magnetic measurements and optical diffuse reflectance spectroscopy. Both hysteresis loops and zero-field-cooling-field-cooling determinations were employed. It was found that a limited solid solution of samarium-doped hematite was formed and the samarium iron perovskite was the end product of the milling performed. The compounds were semiconductors with a band gap of ~2.1 eV.

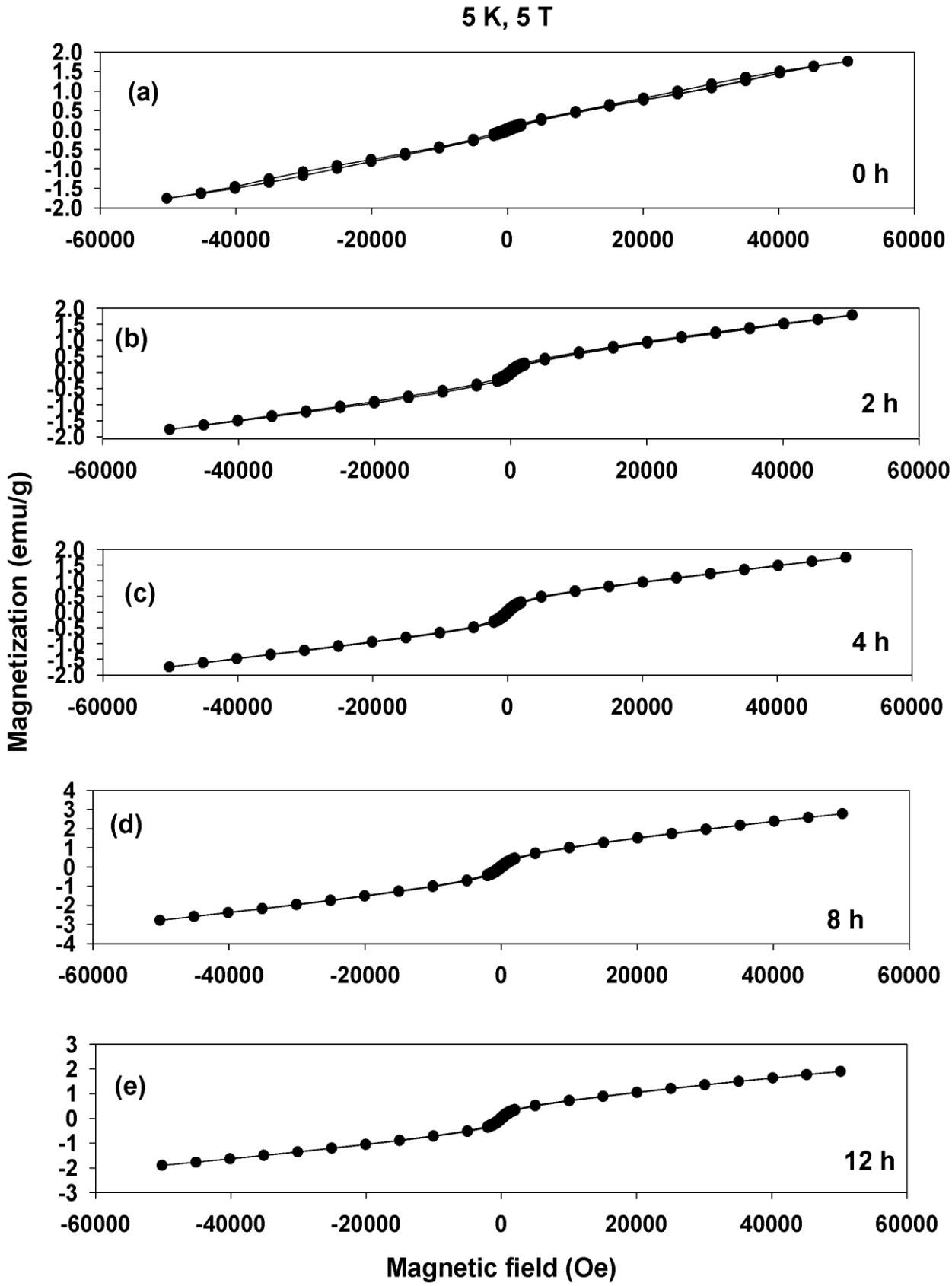

Fig. 4: Hysteresis loops at 5 K and 5 T.

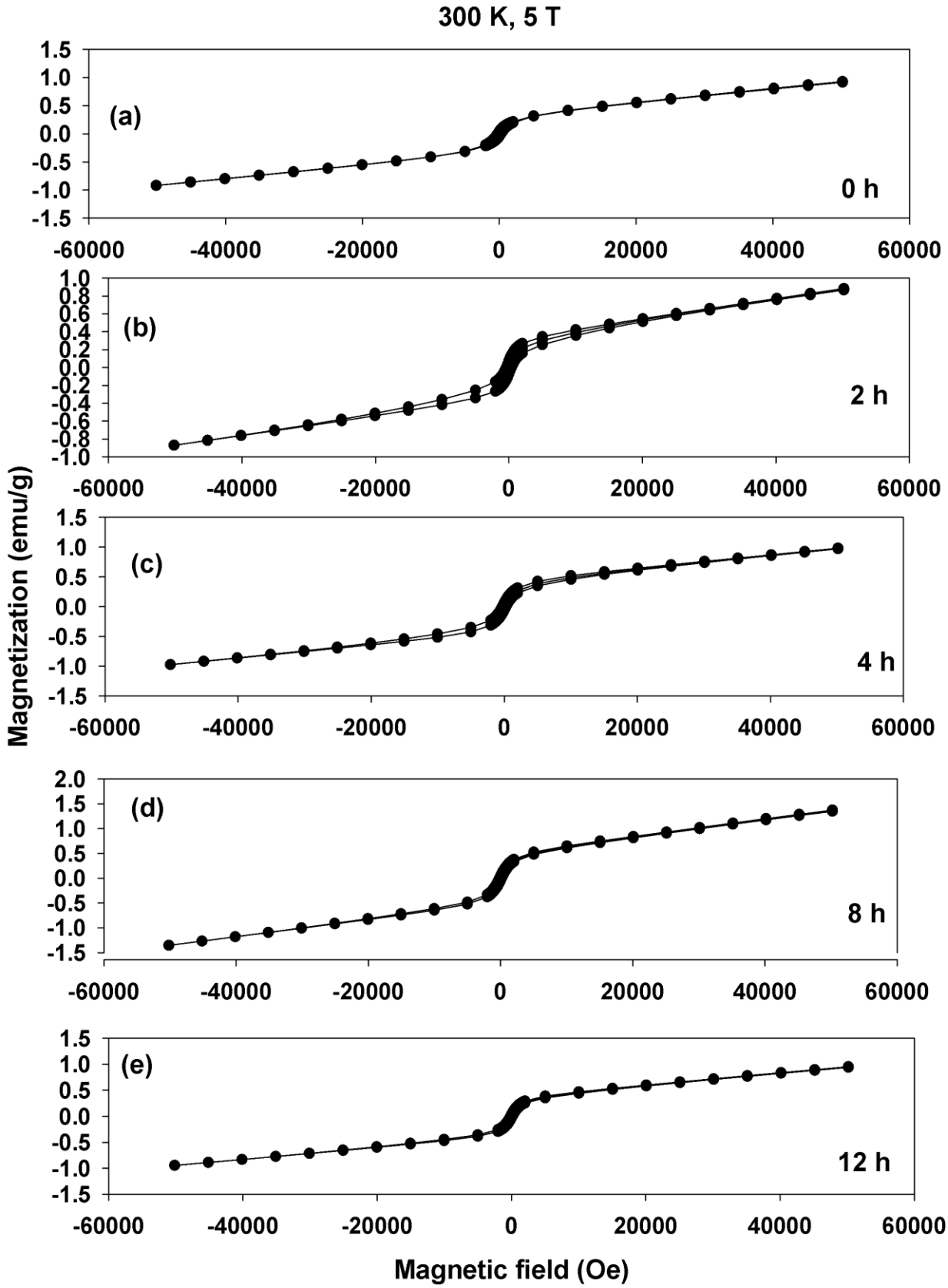

Fig. 5: Hysteresis loops at 300 K and 5 T.

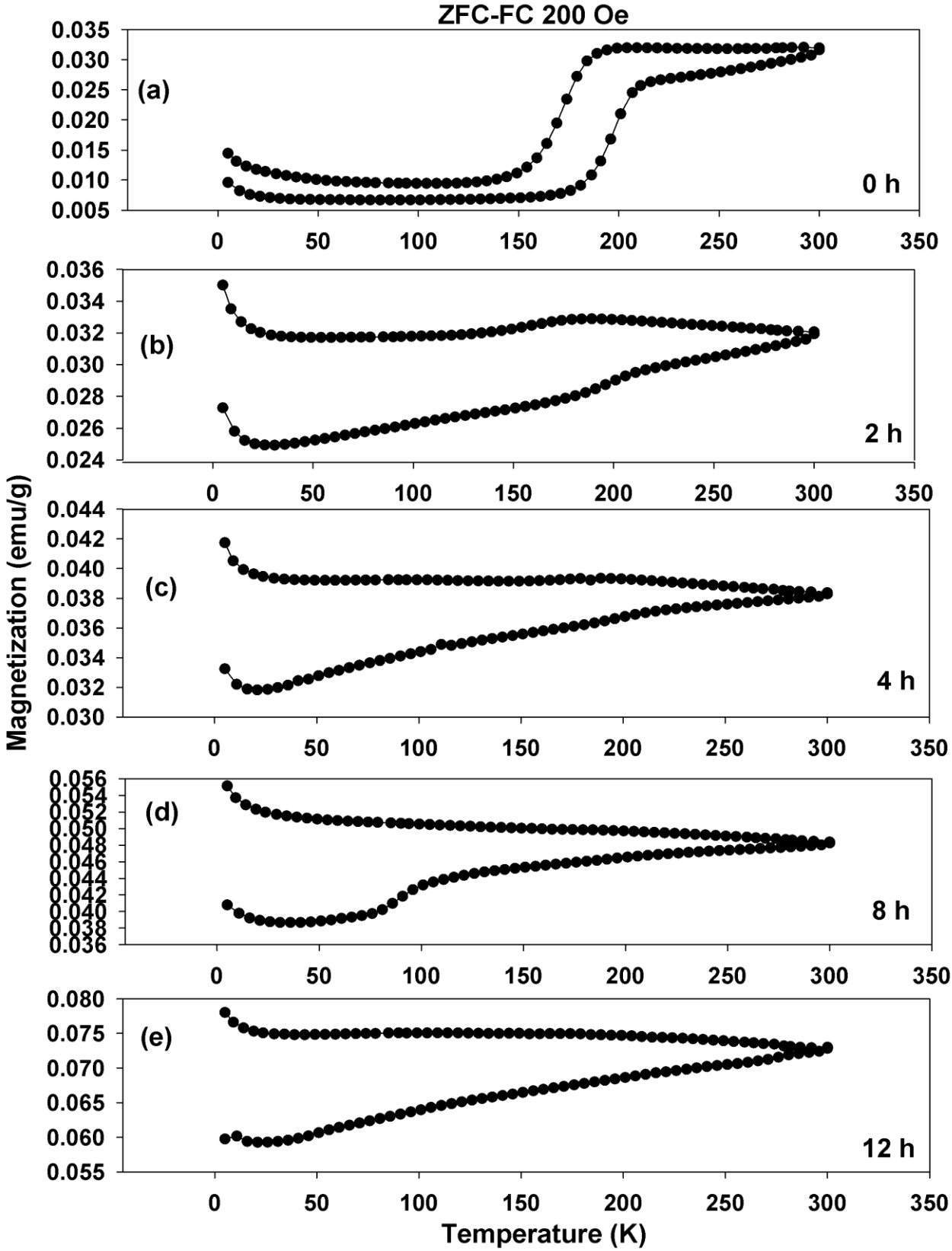

Fig. 6: ZFC-FC curves at 200 Oe and 5-300 K.

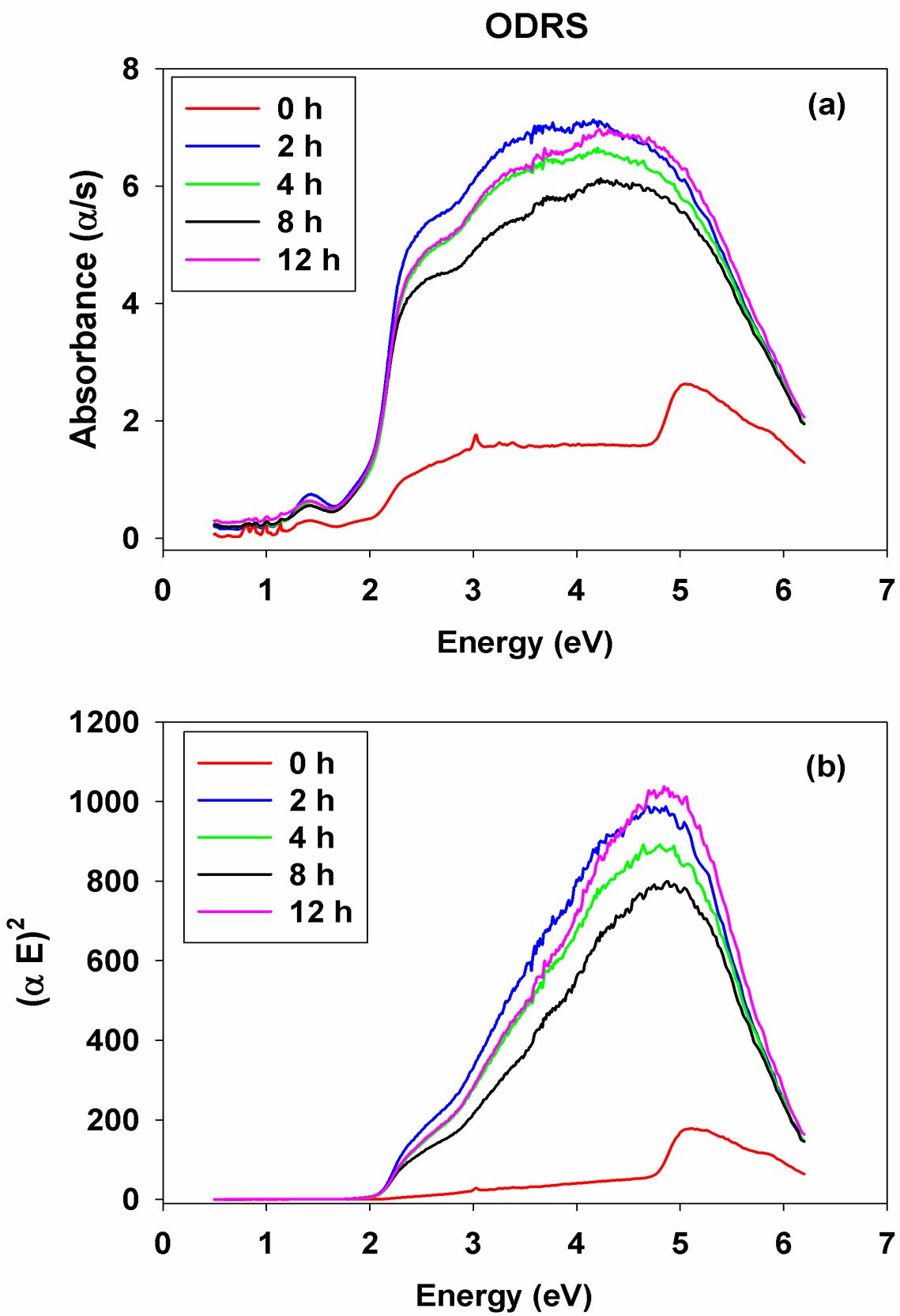

Fig. 7: Optical diffuse reflectance spectra for x=0.5 and BMT of 0-12 h.

ACKNOWLEDGMENT

This work was supported in part by the National Science Foundation, USA under grants number DMR-0854794 and DMR-1002627-1. Funding was also received from the Ministry of Research, Innovation and Digitization (Romania), CNCS/CCCDI-UEFISCDI core program under projects PC2-PN23080202 and 35PFE/2021. J.A.A. and J.C.K. acknowledge the support of the National Science Foundation, USA under grant DMR-1611198. The X-ray powder diffractometer was purchased with funds from the National Science Foundation, USA (DUE-0511444) and an upgrade was financed by the Bayer School of Natural and Environmental Sciences at Duquesne University.

Conflict of Interests

There are no conflicts of interests regarding the work described in this paper.

References

1. Rana, K., et al., *Influence of samarium doping on magnetic and structural properties of M type Ba–Co hexaferrite,* Ceramics International, 2016.42: p.8413-8418. http://dx.doi.org/10.1016/j.ceramint.2016.02.058

2. Srinivasamurthy, K.M., et al., *Evidence of enhanced ferromagnetic nature and hyperfine interaction studies of Ce-Sm doped Co-Ni ferrite nanoparticles for microphone applications,* Ceramics International, 2018.44: p.18878-18885. https://doi.org/10.1016/j.ceramint.2018.07.123

3. Silva, R.L., et al., *Surface effect in PVP coated Sm doped magnetite nanoparticles prepared by the polyol method,* Ceramics International, 2018.44: p.13050-13054. https://doi.org/10.1016/j.ceramint.2018.04.124

4. Tijerina-Rosa, A., et al., *Partial substitution of cobalt by rare-earths (Gd or Sm) in cobalt ferrite: Effect on its microstructure and magnetic properties*, Ceramics International, 2019. 45: p. 22920-22929. https://doi.org/10.1016/j.ceramint.2019.07.335

5. Lin, Q., et al., *Effect of substitution on the structural and magnetic properties of Sm^{3+}- doped / $SmFeO_3$ in nickel-copper-zinc mixed ferrite nanoparticles*, Ceramics International, 2020. 46: p. 2523-2529. https://doi.org/10.1016/j.ceramint.2019.09.246

6. Badapanda, T., et al., *Structural and impedance spectroscopy study of Samarium modified Barium Zirconium Titanate ceramic prepared by mechanochemical route*, Current Applied Physics, 2014. 14: p. 1192-1200. http://dx.doi.org/10.1016/j.cap.2014.06.007

7. Husain, K., et al., *Samarium substituted M-type Ca-hexaferrites: Structural and magnetic features,* Inorganic Chemistry Communications, 2024. 165: 112493. https://doi.org/10.1016/j.inoche.2024.112493

8. Suryanarayana, B., et al., *Effect of Sm^{3+} substitution on dc electrical resistivity and magnetic properties of Ni–Co ferrites*, Journal of the Indian Chemical Society, 2022. 99: 100623. https://doi.org/10.1016/j.jics.2022.100623

9. Romero, M., et al., *Effect of lanthanide on the microstructure and structure of $LnMn_{0.5}Fe_{0.5}O_3$ nanoparticles with Ln=La, Pr, Nd, Sm and Gd prepared by the polymer precursor method,* Journal of Solid State Chemistry, 2015. 221: p. 325-333. http://dx.doi.org/10.1016/j.jssc.2014.10.028

10. Al-Haj, M., *Structural characterization and magnetization of $Mg_{0.7}Zn_{0.3}Sm_xFe_{2-x}O_4$ ferrites,* Journal of Magnetism and Magnetic Materials, 2006. 299: p. 435-439. doi:10.1016/j.jmmm.2005.05.003

11. Nhlapo T.A. and Moyo, T., *The effect of particle size on structural and magnetic properties of Sm^{3+} ion substituted Zn-Mn nanoferrites synthesized by glycol-thermal method*, Journal of Magnetism and Magnetic Materials, 2020. 513: 167096. https://doi.org/10.1016/j.jmmm.2020.167096

12. Shan, S., et al., *Magnetic properties of Sm-doped M-type barium ferrite by high-energy ball mill-assisted solid-phase reaction method,* Journal of Magnetism and Magnetic Materials, 2024. 589: 171558. https://doi.org/10.1016/j.jmmm.2023.171558

13. Zhang, J., et al*., Structural, micro-structure, magnetic and dynamic magneto-elastic properties of samarium-doped nickel-zinc spinel ferrites for efficient power conversion applications,* Journal of Magnetism and Magnetic Materials, 2024. 602: 172176*.* https://doi.org/10.1016/j.jmmm.2024.172176

14. Pakalniskis, A., et al., *Pressure induced phase transitions in Sm-doped $BiFeO_3$ in the morphotropic phase boundary*, Materials Chemistry and Physics, 2022. 277: 125458. https://doi.org/10.1016/j.matchemphys.2021.125458

15. Yuvaraj, S., et al., *Electrical and magnetic properties of spherical $SmFeO_3$ synthesized by aspartic acid assisted combustion method*, Materials Research Bulletin, 2015.72: p. 77-82. http://dx.doi.org/10.1016/j.materresbull.2015.07.013

16. Huizar-Felix, A.M., et al., *Sol–gel based Pechini method synthesis and characterization of $Sm_{1-x}Ca_xFeO_3$ perovskite $0.1 \leq x \leq 0.5$,* Powder Technology, 2012.229: p. 290-293. doi:10.1016/j.powtec.2012.06.057

17. Smith, P.A.I., et al., *Mechanically alloyed Sm-(Co-Fe) permanent magnets*, Scripta Materialia, 1996. 34: p.61-66.

18. J.P. Hos and P.G. McCormick, Mechanochemical synthesis and characterization of nanoparticulate samarium-doped cerium oxide, *Scripta Materialia*, 2003, **48**, 85-90.

19. Dos Santos Bernardino, R.L., et al., *Mechanical alloying synthesis and comprehensive characterization of $SmCoO_3$ perovskite through XRD, XRF, DSC, and UVVis absorbance,* Solid State Sciences, 2024. 151: 107503. https://doi.org/10.1016/j.solidstatesciences.2024.107503

20. Iordanova, N., et al., *Charge transport in metal oxides: A theoretical study of hematite a-Fe_2O_3,* Journal of Chemical Physics, 2005. 122: 144305. https://doi.org/10.1063/1.1869492

21. Rozenberg, G.Kh., et al., *High pressure structural studies of hematite Fe_2O_3*, Physical Review B, 2002*.* 65: 064112. https://doi.org/10.1103/PhysRevB.65.064112

22. Bergenmayer, W., et al., *Ab Initio thermodynamics of oxide surfaces: O_2 on Fe_2O_3 (0001),* Physical Review B, 2004. 69: 195409. https://doi.org/10.1103/PhysRevB.69.195409

23. Zheng, Y., et al., *Quasicubic a-Fe_2O_3 nanoparticles with excellent catalytic performance,* Journal of Physical Chemistry B, 2006. 110: p. 3093-3097. https://doi.org/10.1021/jp056617q

24. Wu, C., et al., *Synthesis of hematite (a-Fe_2O_3) nanorods: Diameter-size and shape effects on their applications in magnetism, lithium ion battery, and gas sensors*, Journal of Physical Chemistry B, 2006. 110: p.17806-17812. doi:10.1021/jp0633906

25. Liu, J.Z., *Morin transition in hematite doped with Iridium ions,* Journal of Magnetism and Magnetic Materials, 1986. 54-57: p. 901-902.

26. Stroh, C., et al., *Ruthenium oxide-hematite magnetic ceramics nanostructures*, Ceramics International, 2015. 41: p. 14367-14375. https://doi.org/10.1016/j.ceramint.2015.07.070

27. Glasser, S., et al., *Effects of mechanochemical activation on the structural, magnetic and optical properties of yttrium iron garnet-graphene nanoparticles*, Physica B, 2023. 650: 414501. doi:10.1016/j.physb.2022.414501

28. Sorescu, M., et al., *Formation of skyrmion phase in the Fe-Co-Si system by mechanochemical activation,* Physica B, 2024. 688: 416153. doi:10.1016/j.physb.2024.416153

29. Glasser, S., et al., *Synthesis and characterization of gadolinium oxide-hematite magnetic ceramic nanostructures,* Journal of Minerals and Materials Characterization and Engineering, 2023. 11: p. 1-15. doi:10.4236/jmmce.2023.111001

30. Sorescu, M., et al., *Mechanochemical synthesis and Mössbauer characterization of neodymium oxide-hematite magnetic ceramic nanoparticles: Phase sequence and recoilless fraction,* Materials Chemistry and Physics, 2022. 277: 125511. https://doi.org/10.1016/j.matchemphys.2021.125511

31. Mora-Ramirez, M.A., et al., *Optical emission bands of Sm_2O_3 and their link with crystalline defects and 4fd↛4fd electronic transitions at UV-Vis region*, Optik, 2021. 241: 167211. doi:10.1016/j.ijleo.2021.167211

32. Tauc, J., et al., *Optical properties and electronic structure of amorphous germanium,* Physica Status Solidi, 1966. 15: p. 627.

33. Mallick, P. and Dash, B.N., *X-ray diffraction and UV-Visible characterizations of a-Fe_2O_3 nanoparticles annealed at different temperature*, Nanoscience and Nanotechnology, 2013. 3: p. 130-134. doi:10.5923/j.nn.20130305.04